A Letters Journal Exploring the Frontiers of Physics

July 2008

EPL, **83** (2008) 10005 www.epljournal.org
doi: 10.1209/0295-5075/83/10005

Wave-number locking in spatially forced pattern-forming systems

R. Manor[1], A. Hagberg[2(a)] and E. Meron[1,3]

[1] *Physics Department, Ben-Gurion University - Beer-Sheva 84105, Israel*
[2] *Mathematical Modeling and Analysis, Theoretical Division, Los Alamos National Laboratory Los Alamos, NM 87545, USA*
[3] *Department of Solar Energy and Environmental Physics, BIDR, Ben Gurion University Sede Boker Campus 84990, Israel*

received 28 February 2008; accepted in final form 19 May 2008
published online 16 June 2008

PACS 05.45.-a – Nonlinear dynamics and chaos
PACS 05.45.Xt – Synchronization; coupled oscillators
PACS 47.54.-r – Pattern selection; pattern formation

Abstract – We use the Swift-Hohenberg model and normal-form equations to study wave-number locking in two-dimensional systems as a result of one-dimensional spatially periodic weak forcing. The freedom of the system to respond in a direction transverse to the forcing leads to wave-number locking in a wide range of forcing wave-numbers, even for weak forcing, unlike the locking in a set of narrow Arnold tongues in one-dimensional systems. Multi-stability ranges of stripe, rectangular, and oblique patterns produce a variety of resonant patterns. The results shed new light on rehabilitation practices of banded vegetation in drylands.

Frequency locking phenomena in temporally forced oscillators are well understood; a forced oscillator can adjust its frequency of oscillation to a rational fraction of the forcing frequency [1] if the mismatch between the two frequencies is small enough. Resonant oscillations of this kind occur in a discontinuous set of intervals (Arnold tongues) along the forcing frequency axis that obeys the Farey hierarchy [2]. Spatially extended oscillatory systems show similar frequency locking behaviors [3–8], but the appearance of a band of long-wavelength modes beyond the oscillatory instability allows for additional instances of frequency locking due to dispersion effects. Resonant standing waves outside the resonance boundaries of uniform oscillations is one example [9–12].

The spatial counterpart of frequency locking, *wave-number locking*, is less well understood. Although much work has been devoted to pattern-forming systems that are subjected to spatially periodic forcing [13–16], including traveling stripe forcing [17], some basic questions of wave-number locking remained largely unexplored. In the simplest setting, wave-number locking can occur in spatially extended systems that go through stationary nonuniform instabilities [18] to stripe patterns and are subjected to time-independent one-dimensional spatially periodic forcing. Wave-number locking in such systems differs from frequency locking in that spatially forced extended systems have the freedom to respond in two and three spatial dimensions, even if the spatial forcing is one-dimensional, while locking in the time domain is inherently one-dimensional. This basic and significant difference has received little attention [19–21].

In this letter we analyze wave-number locking phenomena associated with a *two-dimensional response* to a one-dimensional forcing. We are interested in universal aspects of wave-number locking and therefore base our study on normal-form equations. We derive these equations using a periodically forced Swift-Hohenberg (SH) equation, which helps us motivate the problem and test our analysis using direct numerical solutions. The specific equation we consider is

$$u_t = \varepsilon u - \left(\nabla^2 + k_0^2\right)^2 u - u^3 + (\alpha + \gamma u)\cos(k_f x). \quad (1)$$

In this equation ε is the distance from the instability point of the unforced zero state to a stationary pattern with a wave-number $k_0 \sim O(1)$, k_f is the forcing wave-number, γ is the intensity of multiplicative forcing and α is the intensity of additive forcing.

In the absence of forcing ($\alpha = \gamma = 0$) the unstable zero state $u = 0$ evolves towards a stripe pattern with wave-number k_0, the pattern that minimizes the Lyapunov function of the SH equation (see fig. 1(a)). Applying

(a) E-mail: hagberg@lanl.gov

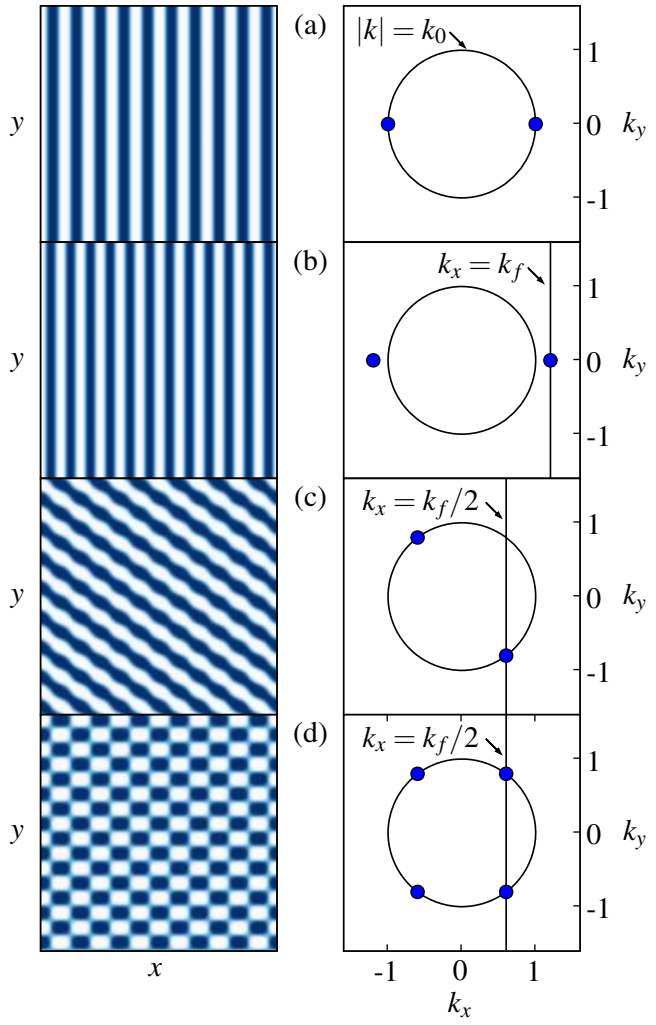

Fig. 1: One- and two-dimensional resonant responses to one-dimensional periodic forcing in the forced SH equation (1). The left frames show the pattern amplitude $u(x, y)$ and the right frames show the maximum in the power spectra for the spatial Fourier transform of u. The circle indicates the ring, $|k| = k_0$, of fastest growing wave-numbers. (a) The unforced system develops a periodic pattern with wave-number $k = k_0$. (b) With additive forcing ($\alpha = 0.05, \gamma = 0$) near the $1:1$ resonance ($k_f = 1.2k_0$) a periodic stripe pattern forms in exact resonance with the forcing $k = k_f$. (c) Multiplicative forcing ($\alpha = 0.0, \gamma = 0.05$) at the same wave-number ($k_f = 1.2k_0$) produces a two-dimensional resonant oblique pattern with $k_x = k_f/2$ in $2:1$ resonance with the forcing. (d) Higher multiplicative forcing ($\gamma = 0.15$) does not induce stripes but instead produces $2:1$ rectangular patterns. Parameters: $\varepsilon = 0.1, k_0 = 1$ on a periodic domain of $x, y = [0, 20\pi]$.

near-resonant additive forcing ($k_f \approx k_0$, $\gamma = 0$, $\alpha > 0$) leads to wave-number locking analogous to frequency locking in forced oscillators; the unstable zero state evolves towards a stripe pattern that adjusts its wave-number k to resonate with the forcing wave-number, $k = k_f$ (fig. 1(b)). However, applying near-resonant multiplicative forcing ($k_f \approx k_0$, $\gamma > 0$, $\alpha = 0$) leads to a *two-dimensional response* in the form of an oblique pattern (fig. 1(c)). The pattern is resonant, because the wave vector component k_x in the x-direction is locked to the forcing wave-number, but the locking ratio is $2:1$, that is, $k_x = k_f/2$ despite the fact that $k_f \approx k_0$. Increasing the forcing intensity γ does not help in recovering the stripe-type pattern of the unforced system, but instead leads to $2:1$ resonant rectangular patterns (fig. 1(d)).

To understand the two-dimensional resonant patterns shown in figs. 1(c) and (d), and to find the parameter ranges for the resonances, we study eq. (1) with multiplicative forcing ($\gamma > 0$, $\alpha = 0$) by deriving normal-form equations for the primary instability of the zero state, $u = 0$. Assuming ε and γ are small, we approximate a solution of eq. (1) in the form [19]

$$u \cong a e^{i(k_x x + k_y y)} + b e^{i(k_x x - k_y y)} + \text{c.c.}, \tag{2}$$

where $k_x = k_0 + \nu = k_f/2$, $k_y = \sqrt{-2k_0\nu - \nu^2}$ and $\nu \sim O(1)$ is a detuning parameter. With this choice $k = \sqrt{k_x^2 + k_y^2} = k_0$, the optimal wave-number that minimizes the Lyapunov function of the Swift-Hohenberg equation. Using the method of multiple scales, assuming a and b vary weakly in space and time, we derive the following equations for the amplitudes a and b [21]:

$$\begin{aligned} a_t &= \varepsilon a + 4(k_x\partial_x + k_y\partial_y)^2 a - 3(|a|^2 + 2|b|^2)a + \frac{\gamma}{2}b^*, \\ b_t &= \varepsilon b + 4(k_x\partial_x - k_y\partial_y)^2 b - 3(|b|^2 + 2|a|^2)b + \frac{\gamma}{2}a^*. \end{aligned} \tag{3}$$

Since eq. (1) is invariant with respect to the transformation $k_f \to -k_f$, we can restrict our analysis to $k_f > 0$, or to ν values satisfying $\nu > -k_0$.

The zero state, $u = 0$, of eq. (1) corresponds to the zero solution $a = b = 0$ of eqs. (3). A linear stability analysis of this solution shows that it becomes unstable to uniform perturbations as ε exceeds $\varepsilon_c = -\gamma/2$. Beyond this threshold resonant rectangular patterns appear, as we will now show.

The condition for resonant solutions of the form (2) is that the amplitudes a and b are independent of x [12]. The simplest solutions of this kind are constant solutions of eqs. (3). Writing the amplitudes in polar forms, $a = \rho_a \exp(i\alpha)$ and $b = \rho_b \exp(i\beta)$, we find the following equivalent dynamic equations for space-independent solutions:

$$\begin{aligned} \rho_{a\,t} &= \varepsilon\rho_a - 3(\rho_a^2 + 2\rho_b^2)\rho_a + \frac{\gamma}{2}\rho_b\cos(\varphi), \\ \rho_{b\,t} &= \varepsilon\rho_b - 3(\rho_b^2 + 2\rho_a^2)\rho_b + \frac{\gamma}{2}\rho_a\cos(\varphi), \end{aligned} \tag{4}$$

and

$$\varphi_t = -\frac{\gamma}{2}\left(\frac{\rho_b}{\rho_a} + \frac{\rho_a}{\rho_b}\right)\sin(\varphi), \tag{5}$$

where $\varphi = \alpha + \beta$. Constant solutions of eqs. (4) and (5) give the following solutions to eq. (4):

$$a_0 = \rho_0 \exp(i\alpha), \qquad b_0 = \rho_0 \exp(-i\alpha), \tag{6}$$

where

$$\rho_0 = \frac{1}{3}\sqrt{\varepsilon + \frac{\gamma}{2}}, \tag{7}$$

and α is an arbitrary constant associated with the continuous symmetry of translations in the y-direction. These solutions describe resonant rectangular patterns. Their existence range is given by $\varepsilon > -\gamma/2$ and $-2k_0 < \nu < 0$ (in order for k_y to be real). Linear stability analysis of these solutions yields the stability condition, $-\gamma/2 < \varepsilon < \gamma$. The same result is obtained by studying the linear stability of these solutions to nonuniform perturbations using eqs. (3). Note that the stability range of rectangular-pattern solutions reduces to zero in the limit of zero forcing, although the solutions continue to exist (provided $\varepsilon > 0$). Equations (3), without the spatial derivative terms, have been derived before in the context of time-periodic forcing of spatially extended oscillatory systems [9]. The rectangular and oblique pattern solutions correspond in that context to standing and traveling wave solutions.

A significant outcome of this analysis is that *rectangular patterns are resonant over a wide and continuous detuning range* $|\nu| \sim O(1)$, despite the fact that the forcing intensity γ can be diminishingly small. This is unlike the Arnold-tongues picture of locking phenomena, where the locking range is small and scales with the forcing intensity. It results from the freedom of the system to build a wave vector component in the y-direction, while keeping the x-component locked to half of the forcing wave-number $k_x = k_f/2$. This finding can be significant for applications where periodic forcing is used as a means of controlling the wave-number of a pattern; adding a second spatial dimension will dramatically increase the range over which the wave-number can be controlled.

What type of pattern solutions appear beyond the instability threshold $\varepsilon = \gamma$ of rectangular patterns? Looking for stationary solutions of eqs. (4) and (5) in the range $\varepsilon > \gamma$, we find two new solution families that bifurcate from the rectangular-pattern solutions:

$$a_\pm = \rho_\pm \exp(i\alpha), \qquad b_\mp = \rho_\mp \exp(-i\alpha), \tag{8}$$

where

$$\rho_\pm = \sqrt{\frac{\varepsilon \pm \sqrt{\varepsilon^2 - \gamma^2}}{6}}, \tag{9}$$

and α is an arbitrary constant. These solutions break the symmetry, $a \to b$, $b \to a$, of eqs. (4), as the bifurcation diagram in fig. 2 shows, and give rise to oblique patterns. They are linearly stable (to uniform and nonuniform perturbations) in the range $\varepsilon > \gamma$, and therefore prevail when the forcing is weak (see fig. 1(c)). Like the rectangular patterns, the oblique patterns are also resonant, because the wave vector component in the forcing direction x is exactly half the forcing wave-number, $k_x = k_f/2$.

The rectangular and oblique patterns cease to exist at $\nu = 0$. This threshold corresponds to 2 : 1 resonant stripe patterns with wave-numbers $k_0 = k_f/2$. The resonance

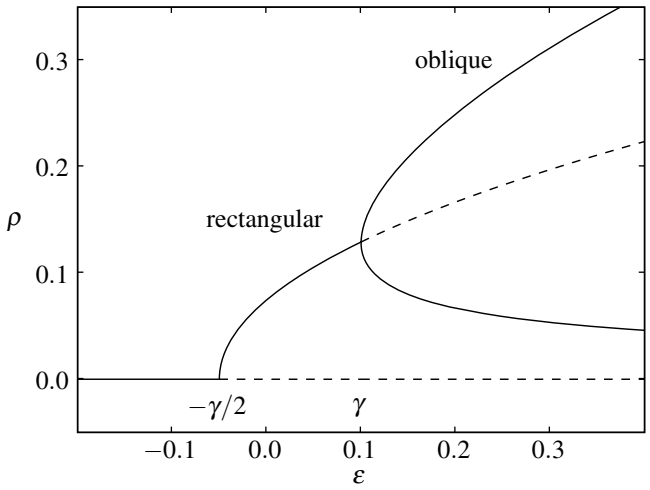

Fig. 2: Bifurcation diagram showing the appearance of rectangular patterns (a_0, b_0) at $\varepsilon = -\gamma/2$ (see eqs. (6) and (7)), and their destabilization to oblique patterns (a_+, b_-) and (a_-, b_+) at $\varepsilon = \gamma$ (see eqs. (8) and (9)).

range of these stripe patterns is expected to widen as γ increases and also to be affected by Eckhaus and zigzag instabilities. To study this range, we approximate stripe solutions of eq. (1) (with $\gamma > 0$ and $\alpha = 0$) by the form

$$u(x,y,t) \cong A(x,y,t) \exp\left(i\frac{k_f}{2}x\right) + \text{c.c.}, \tag{10}$$

where "c.c." stands for the complex conjugate, and derive an equation for the amplitude A, assuming ε, γ and ν are all small. The resulting amplitude equation is

$$A_t = \varepsilon A - \left(2ik_0\partial_x - 2k_0\nu + \partial_y^2\right)^2 A - 3|A|^2 A + \frac{\gamma}{2}A^*. \tag{11}$$

The stationary homogeneous solutions of this equation are given by $A_\pm = \pm\frac{1}{\sqrt{3}}\sqrt{\varepsilon - (2k_0\nu)^2 + \gamma/2}$ and $A_{\pm i} = \pm\frac{i}{\sqrt{3}}\sqrt{\varepsilon - (2k_0\nu)^2 - \gamma/2}$. The former, $A_\pm$, are the first to appear (at $\varepsilon = -\gamma/2 + 4k_0^2\nu^2$) as ε is increased, and are linearly stable to uniform perturbations. The latter, $A_{\pm i}$, are always unstable and will not be discussed any further. To find the stability range of the solutions $A_\pm$, we study their linear stability to nonuniform perturbations of the form $\delta A = a_+ \exp[i(Q_x x + Q_y y)] + a_-^* \exp[-i(Q_x x + Q_y y)]$. This gives the following thresholds for the Eckhaus ($Q_y = 0$) and zigzag ($Q_x = 0$) instabilities:

$$\text{Eckhaus}: \quad \varepsilon = 12k_0^2\nu^2 - 4k_0|\nu|\sqrt{\gamma}, \quad |\nu| > \frac{\sqrt{\gamma}}{4k_0},$$

$$\text{Zigzag}: \quad \varepsilon = 6k_0^2\nu^2 - \gamma/2, \quad \text{or} \quad \nu = -\frac{\sqrt{\gamma}}{2k_0}.$$

These thresholds define the 2 : 1 resonance ranges of stable stripe solutions ($k = k_f/2$). In the limit $\gamma = 0$ these results coincide with the known Eckhaus and zigzag thresholds for the unforced SH equation [18]. The forcing extends the

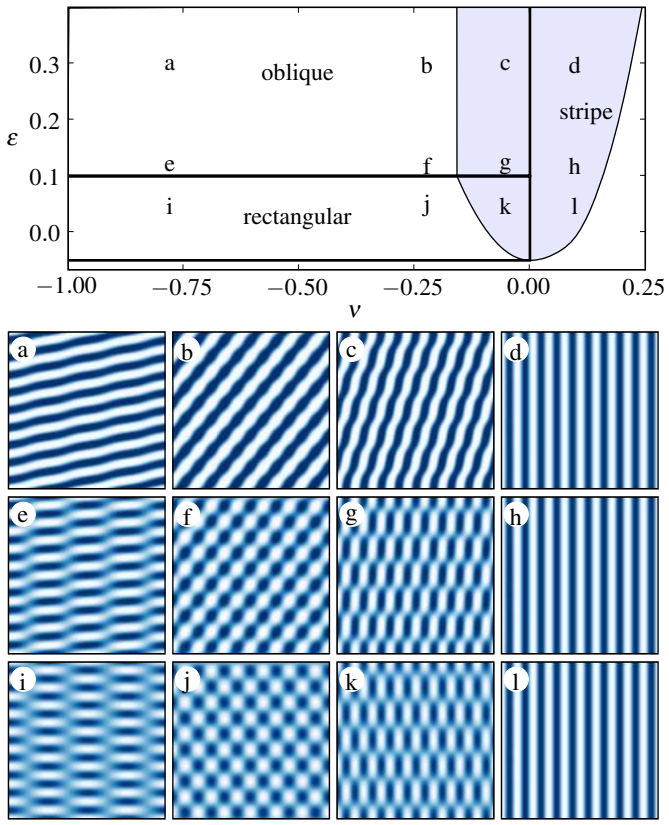

Fig. 3: A narrow resonance range of 2 : 1 stripe patterns ($|\nu| \sim O(\sqrt{\varepsilon})$) *vs.* a wide resonance range of 2 : 1 rectangular and oblique patterns ($|\nu| \sim O(1)$) in the SH model with multiplicative forcing (1). Top: phase diagram in the ν-ε parameter plane showing the regions of stable resonant patterns. Stripes are stable in the shaded region. Stripes and rectangular or oblique patterns coexist for $\nu < 0$ and within the stripe stability region. Bottom: the patterns in (a)–(l) are numerical solutions of eq. (1) with the parameters indicated by the corresponding letter in the phase diagram. Patterns (c), (g), (k) coexist with stable stripe patterns (not shown) at the same parameters. Parameters: $k_0 = 1$, $\alpha = 0$, $\gamma = 0.1$, $\nu = [-0.777, -0.2, -0.05, 0.1]$, $\varepsilon = [0.05, 0.12, 0.3]$.

range of stable stripe solutions to negative ε values, down to the value $\varepsilon = -\gamma/2$ where the rectangular solutions appear. It also extends the range of stable stripes to negative ν values. This implies the existence of bistability ranges of stripe and rectangular patterns for $\varepsilon < \gamma$, and of stripe and oblique patterns for $\varepsilon > \gamma$.

The regimes of all resonant responses discussed so far are displayed in the phase diagram shown in fig. 3. Also shown in this figure are typical forms of stripe, rectangular and oblique patterns, and how they are affected by the detuning ν. Both rectangular and oblique patterns change from stripe patterns along the x-direction, in the limit $\nu \to 0$, to stripe patterns along the y-direction, in the limit $\nu \to -k_0$. Accordingly, the pattern's wave vector component in the x-direction is continuously controllable by the forcing from $k_x = k_0$ ($\nu = 0$) to $k_x = 0$ ($\nu = -k_0$).

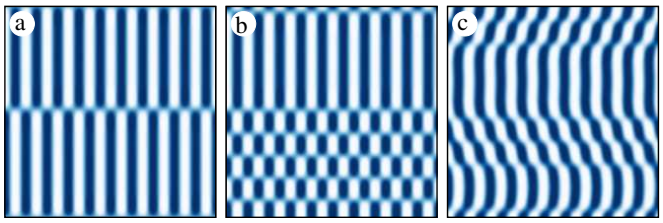

Fig. 4: Resonant mixed patterns with stationary domain walls in multi-stability ranges of pattern states. (a) Phase-shifted stripe patterns separated by a transverse Ising front ($\varepsilon = 0.05$). (b) Mixed stripe and rectangular patterns ($\varepsilon = 0.05$). (c) Mixed stripes and oblique patterns of two different orientations ($\varepsilon = 0.15$). Other parameters: $k_0 = 1$, $\alpha = 0$, $\gamma = 0.1$, $\nu = -0.1$.

At $\nu = -k_0/4$ the rectangular patterns become square patterns and the oblique stripes are exactly diagonal. In the range $\varepsilon \gg \gamma$ the oblique patterns become oblique stripes.

The variety of resonant patterns that can appear in the range $\nu < 0$ is wider than that shown in fig. 3 due to bistability ranges of stripes and rectangular patterns for $\varepsilon < \gamma$, and tristability ranges of stripes and the two symmetric oblique patterns for $\varepsilon > \gamma$. In the range $\varepsilon < \gamma$ asymptotic spatial mixtures of stripe and rectangular patterns are found whenever the domain walls that separate the two patterns are perpendicular to the stripe direction. Such domain walls are close approximations of stationary transverse Ising fronts [22]. Domain walls aligned parallel to the stripes propagate to reduce and eliminate stripe domains, leaving an asymptotic rectangular pattern. Fronts may also form between stripes and oblique patterns but in that case the fronts may be either aligned perpendicular or parallel to the stripes. Figure 4 shows examples of resonant patterns consisting of mixtures of stripe, rectangular, and oblique patterns.

The results predicted here can be tested by controlled experiments in a Rayleigh-Bénard convection system which is spatially forced by periodic modulation of the bottom plate [23]. A possible ecological application for these results is the rehabilitation of banded vegetation in arid and semi-arid regions. Vegetation on hill slopes often self-organizes to form stripe patterns oriented perpendicular to the slope direction [24,25]. Recovery practices of degraded vegetation are based on water-harvesting methods such as parallel contour ditches that accumulate runoff and along which the vegetation is planted. The contour ditches increase the biomass growth rate because of the higher soil-water densities they induce [26,27], and therefore can be regarded as multiplicative periodic forcing. The results shown in fig. 1(c) and (d) then suggest that this practice may lead to two-dimensional vegetation patterns rather than vegetation stripes, and consequently to lower bio-productivity (2 : 1 resonance instead of the intended 1 : 1 resonance).

* * *

The support of the James S. McDonnell Foundation is gratefully acknowledged. Part of this work was funded by the Department of Energy at Los Alamos National Laboratory under contract DE-AC52-06NA25396, and the DOE Office of Science Advanced Computing Research (ASCR) program in Applied Mathematical Sciences.

REFERENCES

[1] Arnold V. I., *Geometrical Methods in the Theory of Ordinary Differential Equations* (Springer-Verlag, New York) 1983.
[2] Hao B.-L., *Elementary Symbolic Dynamics and Chaos in Dissipative Systems* (World Scientific, Singapore) 1989.
[3] Coullet P. and Emilsson K., *Physica D*, **61** (1992) 119.
[4] Chaté H., Pikovsky A. and Rudzick O., *Physica D*, **131** (1999) 17.
[5] Petrov V., Ouyang Q. and Swinney H. L., *Nature*, **388** (1997) 655.
[6] Walgraef D., *Spatio-Temporal Pattern Formation* (Springer-Verlag, New York) 1997.
[7] Lin A. L., Bertram M., Martinez K., Swinney H. L., Ardelea A. and Carey G. F., *Phys. Rev. Lett.*, **84** (2000) 4240.
[8] Lin A. L., Hagberg A., Meron E. and Swinney H. L., *Phys. Rev. E*, **69** (2004) 066217.
[9] Riecke H., Crawford J. D. and Knobloch E., *Phys. Rev. Lett.*, **61** (1988) 1942.
[10] Park H.-K., *Phys. Rev. Lett.*, **86** (2001) 1130.
[11] Yochelis A., Hagberg A., Meron E., Lin A. L. and Swinney H. L., *SIAM J. Appl. Dyn. Syst.*, **1** (2002) 236.
[12] Yochelis A., Elphick C., Hagberg A. and Meron E., *Europhys. Lett.*, **69** (2005) 170.
[13] Lowe M., Gollub J. P. and Lubensky T. C., *Phys. Rev. Lett.*, **51** (1983) 786.
[14] Dolnik M., Berenstein I., Zhabotinsky A. M. and Epstein I. R., *Phys. Rev. Lett.*, **87** (2001) 238301.
[15] Schmitz R. and Zimmermann R. W., *Phys. Rev. E*, **53** (1996) 5993.
[16] Peter R., Hilt M., Ziebert F., Bammert J., Erlenkämper C., Lorscheid N., Weitenberg C., Winter A., Hammele M. and Zimmermann W., *Phys. Rev. E*, **71** (2005) 046212.
[17] Míguez D. G., Nicola E. M., Muñuzuri A. P., Casademunt J., Sagués F. and Kramer L., *Phys. Rev. Lett.*, **93** (2004) 048303.
[18] Cross M. C. and Hohenberg P. C., *Rev. Mod. Phys.*, **65** (1993) 851.
[19] Kelly R. E. and Pal D., *J. Fluid Mech.*, **86** (1978) 433.
[20] Pismen L. M., *Phys. Rev. Lett.*, **59** (1987) 2740.
[21] Zimmermann W., Ogawa A., Kai S., Kawasaki K. and Kawakatsu T., *Europhys. Lett.*, **24** (1993) 217.
[22] Korzinov L., Rabinovich M. I. and Tsimring L. S., *Phys. Rev. A*, **46** (1992) 7601.
[23] McCoy J., *Adventures in Pattern Formation: Spatially Periodic Forcing and Self-Organization*, PhD Thesis, Cornell University (2007).
[24] Valentin C., d'Herbès J. M. and Poesen J., *Catena*, **37** (1999) 1.
[25] Yizhaq H., Gilad E. and Meron E., *Physica A*, **356** (2005) 139.
[26] von Hardenberg J., Meron E., Shachak M. and Zarmi Y., *Phys. Rev. Lett.*, **87** (2001) 198101.
[27] Gilad E., von Hardenberg J., Provenzale A., Shachak M. and Meron E., *Phys. Rev. Lett.*, **93** (2004) 098105.